POD analysis of the recovery process in wind turbine wakes

Giovanni de Cillis, Stefania Cherubini, Onofrio Semeraro, Stefano Leonardi, Pietro de Palma

POD analysis of the recovery process in wind turbine wakes

POD analysis of the recovery process in wind turbine wakes

G De Cillis[1,2], S Cherubini[1], O Semeraro[3], S Leonardi[2] and P De Palma[1]

[1] Department of Mechanics, Mathematics and Management, Politecnico di Bari, Italy
[2] Department of Mechanical Engineering, University of Texas at Dallas, Texas, USA
[3] LIMSI,CNRS, Université de Paris-Saclay, France

E-mail: giovanni.decillis@poliba.it

Abstract. The wake produced by a single three-bladed wind turbine is investigated using the proper orthogonal decomposition (POD) of numerical data obtained by a large eddy simulation. The rotor blades are modeled using the actuator line method, whereas tower and nacelle are simulated through an immersed boundary method. The POD is performed in a three-dimensional subdomain enclosing the wake after conducting a convergence test, which demonstrates that the first ten modes are well converged. Most energetic POD modes identify and isolate different flow features characterising the wake dynamics, such as the tip-vortices spirals, the von Kármán vortices shed by the tower, the Kelvin-Helmholtz instability linked to the wake shear layer. Very low frequency modes are also found, which could be related to the wake meandering phenomenon. Moreover, the wake recovery process is studied by computing the contribution of each POD mode to the mean-kinetic-energy entrainment. This analysis indicates that tip vortices negatively affect the wake recovery, since they provide a negative entrainment. On the contrary, flow structures related to the tower wake are found to be beneficial to wake recovery, demonstrating the importance of including tower and nacelle in numerical simulations.

1. Introduction

Harnessing wind energy and converting it in electric energy require the design and installation of large wind farms, constituted by hundreds of turbines. When grouped together, a great part of the wind turbines operates in the wake of upwind turbines, so that the velocity deficit and the turbulence level of the incoming flow induce additional power losses and fatigue blade loading [1–3]. Thus, understanding the dynamics of wind turbine wakes is crucial for the design and efficiency improvement of wind turbines and farms. This task is challenging, considering that the main features of atmospheric turbulence may spread over a wide range of spatial and time scales [4]. Thus, a possible approach is to simplify the problem by focusing on the study of the dynamics of a single wake.

Typically, the part of the wake close to the turbine (near wake) is characterized by vortex structures shed from the tip and the root of the rotor blade (namely, the tip- and root-vortices) which become unstable and break down forming small-scale turbulent structures. At the center of the near wake, a hub vortex is formed, elongated in the streamwise direction [5, 6]. The far wake, instead, is characterized by turbulent structures derived from the break-down of coherent vortices and by the entrainment of the outer flow, up to wake recovery [7, 8]. How these coherent structures in the near and far wake contribute to wake recovery, is however still an open problem.

The present work provides an analysis of the dynamics and recovery of the wake of a wind turbine using the proper orthogonal decomposition (POD) technique [9, 10] applied to numerical data obtained by large

eddy simulation (LES). Such a technique has been recently introduced in the study of wind turbines and wind farms. VerHulst and Meneveau [11] applied this technique to the study of a wind farm. They found four different families of POD modes, and determined the number of POD modes necessary to capture most of the turbulent kinetic energy of the flow. Sarmast et al. Ivanell et al. [12] and then Sarmast et al. [13] discussed the stability of the tip vortices, by analysing the mechanisms leading to vortex pairing using large eddy simulations. Bastine et al. [14, 15] performed a two-dimensional POD analysis using LES data of the wake of a wind turbine, considering an incoming turbulent athmospheric boundary layer. Hamilton et al. [16] investigated wake interaction and recovery dynamics using POD applied to velocity measurements. Sorensen et al. [17] applied POD on the LES results for a single-turbine wake. Debnath et al. [18] studied the dynamics of wind turbine wakes and instabilities of helicoidal tip vortices using three-dimensional POD.
Most of these works neglect the contribution of tower and nacelle to the flow dynamics, in order to simplify the problem. However, we are going to show that the influence of tower and nacelle is fundamental for the dynamics of the wake and for correctly estimating its recovery. The present work provides a POD analysis of a wind turbine wake, based on a full three-dimensional set of data obtained by an LES. A complete turbine geometry is considered, including the tower and the nacelle. We focus on the analysis of the coherent structures in the wake, in order to study the basic mechanisms of wake recovery.

2. Methodology

2.1. Large Eddy Simulation (LES)

In the present work an LES is performed in order to investigate the dynamics of the wake developing behind a wind turbine. LES is based on the solution of the filtered Navier-Stokes equations, by which only the large-scale structures of the flow are computed, down to a certain cut-off length scale. Small-scale structures are filtered out and their effect on the resolved scales is modeled [19]. The governing equations for the filtered non-dimensional velocity, $\boldsymbol{u}$, and pressure, p, derived from the Navier-Stokes equations for incompressible flows read as follow:

$$\frac{\partial u_i}{\partial t} + \frac{\partial u_i u_j}{\partial x_j} = -\frac{\partial p}{\partial x_i} + \frac{1}{Re}\frac{\partial^2 u_i}{\partial x_j \partial x_j} - \frac{\partial \tau_{ij}}{\partial x_j} + f_i, \tag{1}$$

$$\frac{\partial u_i}{\partial x_i} = 0, \tag{2}$$

where $i, j \in \{1, 2, 3\}$ indicate the components in the Cartesian reference frame corresponding to the streamwise, x, wall-normal, y, and spanwise, z, directions, respectively. The Reynolds number is defined as $Re = {}^{U_\infty D}/_{\nu}$, where U_∞ is the inlet velocity, D is the rotor diameter and ν is the kinematic viscosity of the fluid, which have been used as reference variables (namely, $x = {}^{X}/_{D}, y = {}^{Y}/_{D}, z = {}^{Z}/_{D}$ and $u_i = {}^{U_i}/_{U_\infty}$). The subgrid-scale stress tensor, τ_{ij}, can be decomposed into an isotropic part and an anisotropic part, τ^r_{ij}. The isotropic part is included in the modified filtered pressure $p^* = p + \frac{1}{3}\tau_{ii}$, whereas the anisotropic part needs to be modeled. The Smagorinsky model is employed in the present work, with the Smagorinsky constant C_S set to 0.09.
The last term in equation (1), f_i, is the force per unit volume which models the aerodynamic forces exerted by the turbine blades on the fluid via the actuator line method, as will be explained in sub-section 2.2. The governing equations are solved using a second-order-accurate centered finite difference scheme on a staggered Cartesian grid and an hybrid low-storage third-order-accurate Runge-Kutta scheme for time integration [20].

2.2. Actuator line and immersed boundary methods

Rotor blades are simulated employing the actuator line method (ALM) proposed by Sørensen & Shen [21]. This method relies on the estimate of the forces exerted by the blades on the fluid on the basis of

tabulated data providing the two-dimensional performance of blade's airfoils at each radius, namely the lift, C_L, and drag, C_D, coefficients. Each blade is treated as a rotating rigid line, which is divided into discrete segments. Given the chord, c, and twist-angle, ϕ, distributions along the blade radius, as well as the fluid density ρ, the lift and drag forces per unit length for each segment are estimated as follows:

$$F_L = \frac{1}{2}\rho u_{rel}^2 C_L(\alpha) c F, \tag{3}$$

$$F_D = \frac{1}{2}\rho u_{rel}^2 C_D(\alpha) c F, \tag{4}$$

where u_{rel} is the relative inflow velocity and α is the angle of attack. The coefficient F is a modified Prandtl correction factor [22], which accounts for performance degradation due to tip and root vortices. The calculated aerodynamic forces, F_L and F_D, are spread on areas perpendicular to each actuator line with a Gaussian distribution kernel.

The tower and nacelle are described using the immersed boundary method [23, 24], which avoids the use of a body-fitted grid, reducing the computational cost of the simulations. In particular, a discrete forcing approach, in which the forcing is introduced in the discretised equations, similar to the approach proposed by Orlandi & Leonardi [24], has been used.

2.3. POD

The Proper Orthogonal Decomposition (POD) is a statistical approach providing the optimal orthogonal basis, in terms of kinetic energy, for the flow dynamics. The POD modes are ranked according to their energy and the most energetic ones are mostly related to large organised structures. Therefore, the POD represents a useful tool for the analysis of experimental as well as numerical (DNS, LES) data, providing the most energetic coherent structures characterising the flow.

The POD is based on the eigendecomposition of the two-point spatial correlation tensor C, where the eigenvectors represent the POD modes, whereas the associated eigenvalues represent their energy. A good approximation of the tensor C, based on data, requires a large number M of snapshots of the flow field, which can be organised into a single matrix $\mathbf{Q} \in \mathbb{R}^{N \times M}$, each column being a single instantaneous velocity field, represented by N scalars.

$$\mathbf{Q} = \begin{bmatrix} | & | & | & & | \\ \mathbf{q}^1 & \mathbf{q}^2 & \mathbf{q}^3 & \dots & \mathbf{q}^M \\ | & | & | & & | \end{bmatrix}. \tag{5}$$

Assuming that all snapshots are equally spaced in time, the two-point correlation tensor can be approximated by the matrix $\mathbf{C} \in \mathbb{R}^{N \times N}$ given by the product of the snapshot matrix $\mathbf{Q}$ by its transpose, divided by the total number of snapshots.

$$\mathbf{C} = \frac{1}{M}\mathbf{Q}\mathbf{Q}^T \tag{6}$$

The POD can then be easily performed by computing the singular value decomposition of the snapshot matrix $\mathbf{Q}$, divided by the square root of the number of snapshots M,

$$\frac{\mathbf{Q}}{\sqrt{M}} = \mathbf{\Phi}\mathbf{\Sigma}\mathbf{\Psi}^T, \tag{7}$$

where the columns $\boldsymbol{\phi}_k$ of the matrix $\mathbf{\Phi}$ correspond to the right eigenvectors of $\mathbf{C}$, namely to the POD modes, and the eigenvalues $\mathbf{\Lambda}$ of $\mathbf{C}$ are equal to the singular values squared, namely $\mathbf{\Lambda} = \mathbf{\Sigma}^2$. The time series considered can then be expanded as:

$$\mathbf{q}^i = \sum_{k=1}^{M} \mathrm{a}_k(t_i)\boldsymbol{\phi}_k \tag{8}$$

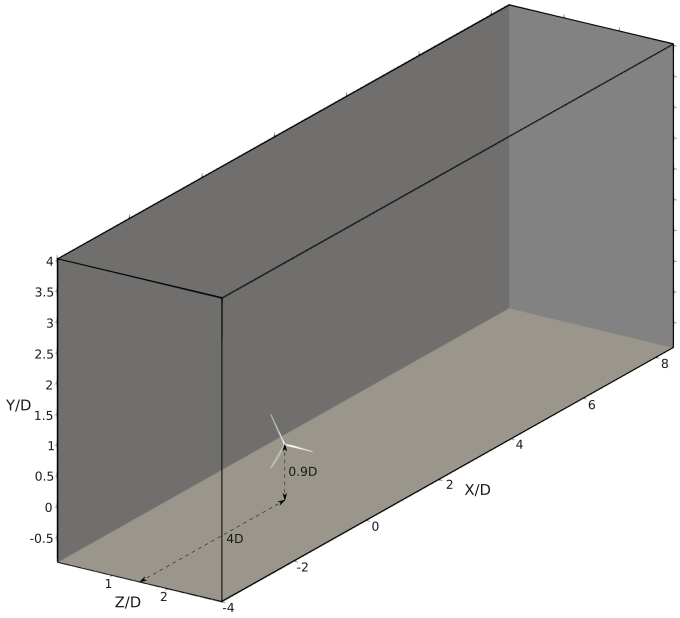

Figure 1: Computational box employed in the simulations.

where the time coefficients of each POD mode, a_k, are given by the rows of the matrix $\sqrt{M}\mathbf{\Sigma}\mathbf{\Psi}^T$. In addition, it can be shown that the time coefficients a_k are uncorrelated at zero time-lag:

$$\overline{\mathrm{a}_j \mathrm{a}_k} = \lambda_j \delta_{jk} \tag{9}$$

3. Simulation setup

The case under investigation is that of a three bladed wind turbine of diameter D, invested by a uniform axial velocity U_∞, rotating at a constant tip-speed ratio $\lambda = 3$ at the Reynolds number $Re = 6.3 \times 10^5$. The rotor axis is located at $y_h = 0.914D$ above the ground. The tower and the nacelle are modeled as cylinders with diameter $d_t = 0.1D$, the second having an axial length of $0.3D$. The computational domain has dimensions $12.5D \times 5D \times 3D$ in the streamwise (x), vertical (y) and transverse (z) directions, respectively. The turbine is located at $4D$ from the inlet, where a uniform velocity U_∞ is imposed, and it is centered in the transverse direction. A radiative boundary condition is employed at the outlet with uniform convection velocity $C = 0.9$ [25]. No-slip and free-slip conditions are imposed at the bottom- and the top-wall, respectively, whereas the lateral boundaries are periodic. The computational grid used consists of $2048 \times 512 \times 512$ grid-points in x,y and z directions, respectively. The grid is uniform along the streamwise and spanwise directions, whereas it is stretched in the vertical direction, with finer (uniform) spacing in the lower part of the domain, where the turbine's wake will develop.

4. POD convergence

The convergence of the computed POD modes has been assessed considering several dataset composed of an increasing number of snapshots. The eigenvalues spectra obtained for each dataset are compared. Moreover, the spectral contents of the time coffiecients, $\mathrm{a}_k(t)$, obtained from each dataset are analysed and compared in order to check if the computed dynamics is independent of the number of snapshots. Seven dataset made by $M = \{1500; 1650; 1800; 1950; 2100; 2250; 2361\}$ snapshots, have been considered. Figure 2 shows that a good convergence is reached up the 19^{th} mode. Welch's spectra relative to the first six POD pairs ($k = 2i, i = 1, 6$) are shown in figure 3. It can be observed that the first five pairs of modes already converged for $M = 1500$, showing small variation of their spectral content for larger numbers of snapshots; whereas the sixth pair (12^{th} mode) begins to converge at $M = 1800$.

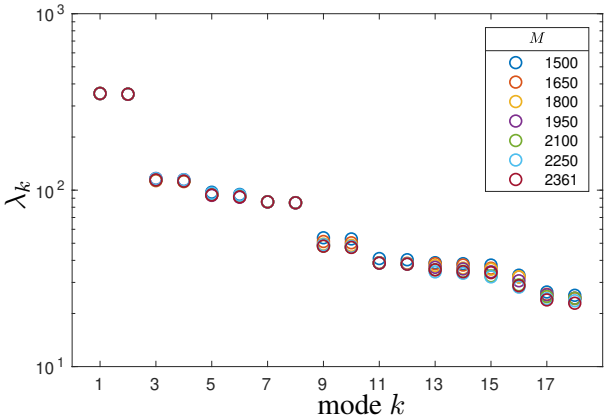

Figure 2: Eigenvalues associated to the most energetic POD modes using different dataset with increasing number of snapshots M (see legend).

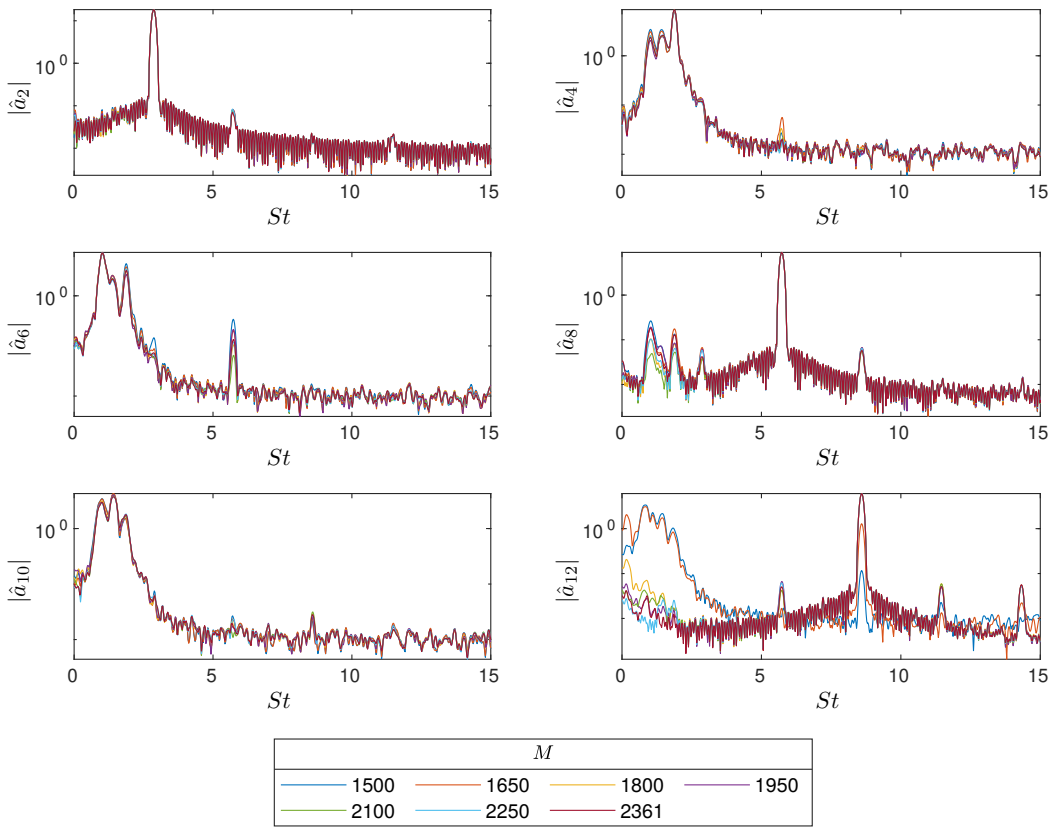

Figure 3: Welch's spectra relative to the first six POD pairs of modes ($k = 2i, i = 1, 6$) with increasing number of snapshots M (see legend).

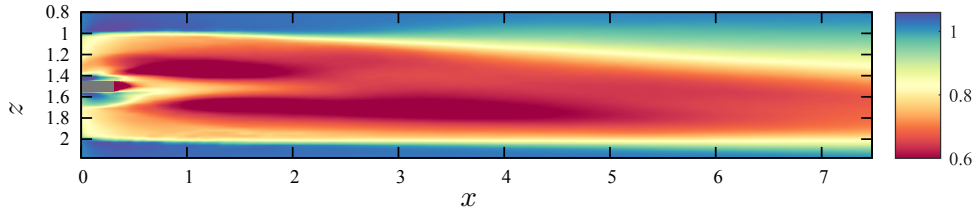

Figure 4: Streamwise velocity of the 0^{th}mode multiplied by a_0 at $y = 0$.

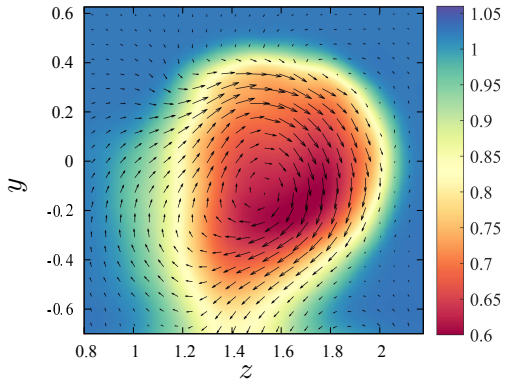

Figure 5: Streamwise velocity of the 0^{th}mode multiplied by a_0 at $x = 5$.

5. Results

The POD analysis provided in this section is carried out on a dataset composed of $M = 2361$ snapshots of the velocity field, stored every 10° rotation, in a sub-domain enclosing the wake with dimensions $[0\ 7.5] \times [-0,7\ 0.63] \times [0.8\ 2.2]$, where the velocities have been downsampled with a 1:5 ratio with respect to the computational grid.

5.1. POD modes Analysis

The 0^{th} POD mode represents the time-averaged flow, shown in horizontal and vertical planes in figures 4 and 5, respectively. In both planes the asymmetry of the wake is evident; in particular, a faster recovery of the wake is observed on the left side of the wake as can be seen in the left part of the z-y plane in figure 5, corresponding to the top side of the x-z plane in figure 4. The first 12 POD modes, which represent approximately the 25% of the turbulent kinetic energy, are provided in figure 6 in x-z planes, at different y-locations, depending on the mode dynamics. It can be observed, by looking at the modes' structure, that the first 10 POD modes are paired. Different physical mechanisms are isolated by means of the POD analysis: the first pair (figure 6(a, b)) represents the tip/root-vortex helical system; the second pair (figure 6(c, d)) is related to the von Karman street shed by the tower; the third pair (figure 6(e, f)) represents a harmonic of the tip- and root-vortices; the fourth pair (figure 6(g, h)) is still connected to the tower's vortices, but it also shows lower-frequency oscillations far from the rotor, which can be originated from a non-linear interaction between von Karman vortices and tip-vortices spirals; the fifth pair (figure 6(i, j)) appears to be a Kelvin-Helmholtz-like instability, since it is located right at wake mean-flow shear layer, following the same tilted direction; the last two modes (figure 6(k, l)) are not paired and show quite lower frequencies with respect to the other modes. These two modes could be associated to the wake meandering phenomenon.

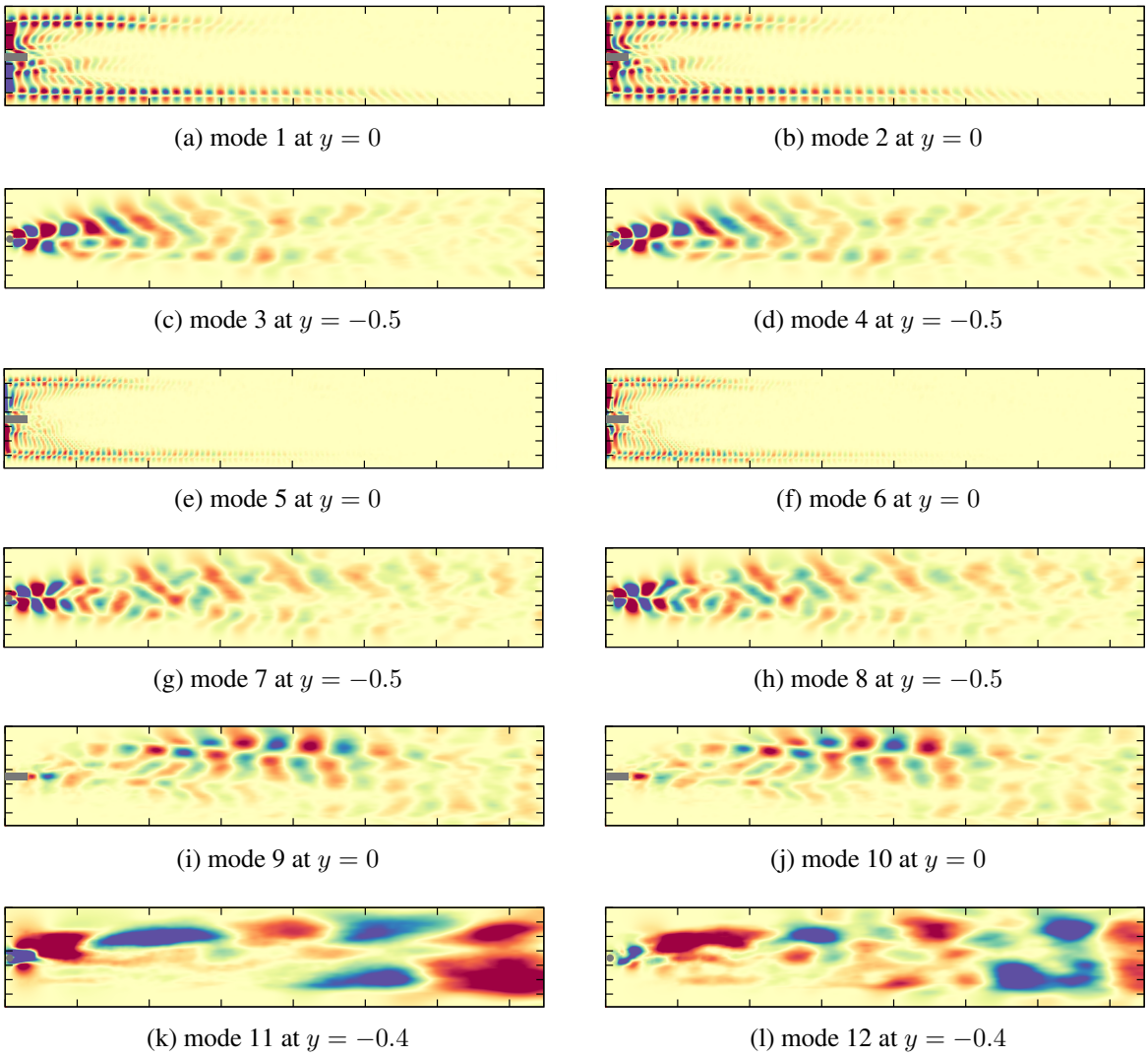

(a) mode 1 at $y = 0$ (b) mode 2 at $y = 0$

(c) mode 3 at $y = -0.5$ (d) mode 4 at $y = -0.5$

(e) mode 5 at $y = 0$ (f) mode 6 at $y = 0$

(g) mode 7 at $y = -0.5$ (h) mode 8 at $y = -0.5$

(i) mode 9 at $y = 0$ (j) mode 10 at $y = 0$

(k) mode 11 at $y = -0.4$ (l) mode 12 at $y = -0.4$

Figure 6: Streamwise velocity contours of the first twelve POD modes.

5.2. Kinetic energy entrainment

It is well established that high turbulence levels in the wake region promote the recovery of the wake, as a result of turbulent flux of mean kinetic energy (M.K.E.). In the present work we aim at evaluating the effect of each POD mode, associated to a specific physical mechanism, on the recovery of the wake. At this purpose, the following equation, governing the M.K.E. transport, is considered:

$$0 = -\bar{u}_j \frac{\partial}{\partial x_j}\left(\frac{1}{2}\bar{u}_i\bar{u}_i\right) - \frac{\partial}{\partial x_i}(\bar{u}_i p^*) + \bar{u}_i \bar{f}_i + \frac{1}{Re}\nabla^2\left(\frac{1}{2}\bar{u}_i\bar{u}_i\right) - \frac{1}{Re}\frac{\partial \bar{u}_i}{\partial x_j}\frac{\partial \bar{u}_i}{\partial x_j} + \underbrace{-\frac{\partial}{\partial x_j}\left(\bar{u}_i\overline{u_i'u_j'}\right) - \frac{\partial}{\partial x_j}\left(\bar{u}_i\overline{\tau_{ij}^r}\right)}_{\text{Turbulent M.K.E. flux}} + \overline{u_i'u_j'}\frac{\partial \bar{u}_i}{\partial x_j} + \overline{\tau_{ij}^r}\frac{\partial \bar{u}_i}{\partial x_j}. \tag{10}$$

As already mentioned, several authors [11, 26] showed that the M.K.E. recovery in the wake is mostly due to the turbulent M.K.E. flux, highlighted in the equation (10). Since the term related to the subgrid-scale stresses is negligible with respect to the Reynolds stresses in the wake region, only the latter are

considered. Taking advantage of the Stokes theorem, it is possible to compute the turbulent M.K.E. net flux per unit area, through a cylindrical surface S of radius $R = 0.5$ enclosing the wake, according to the equation

$$\mathcal{F}_T = \frac{1}{S}\int_S -\bar{u}_i\overline{u_i' u_j'}dS_j. \tag{11}$$

The vector representing the infinitesimal surface element $\boldsymbol{dS}$ is normal to the streamwise direction, therefore it can be expressed in Cartesian coordinates as:

$$\boldsymbol{dS} = (0, dc_2, dc_3)\, dx, \tag{12}$$

where dc_2 and dc_3 are the components in the wall-normal and spanwise directions, respectively, of the vector $\boldsymbol{dc}$ normal to the infinitesimal arc of the cylinder circumference C. Given the POD properties described in section 2.3, the Reynolds stress tensor can be decomposed as:

$$\overline{u_i' u_j'} \approx \overline{\sum_{k=1}^{M}(\mathrm{a}_k\phi_i^k)\sum_{l=1}^{M}(\mathrm{a}_l\phi_j^l)} = \sum_{k=1}^{M}\sum_{l=1}^{M}\overline{\mathrm{a}_k\mathrm{a}_l}\phi_i^k\phi_j^l = \sum_{k=1}^{M}\lambda_k\phi_i^k\phi_j^k. \tag{13}$$

Using this decomposition, one can compute the contribution of each POD mode to the turbulent M.K.E. flux as:

$$\mathcal{F}_T^k = \frac{1}{S}\int_S -\bar{u}_i\lambda_k\phi_i^k\phi_j^k dS_j. \tag{14}$$

The histogram in figure 7 shows the flux $\mathcal{F}_T^k$ for the first 12 POD modes. It is interesting to notice that the POD modes related to the tip vortices, namely modes 1, 2, 5 and 6, provide a negative flux of mean kinetic energy, having therefore an adverse effect on wake recovery. However, this is reasonable because the tip vortices induce a negative streamwise velocity within the wake, playing a crucial role on the generation of the wake itself [27]. An idea of the velocity induced by the tip vortices can be gained by looking at the vector field in figure 8, which is obtained using to the following equation:

$$\mathbf{u}_{TV} = \sum_{k=0}^{2}\mathrm{a}_k(t_1)\phi_k - U_\infty. \tag{15}$$

The figure clearly show that the rotation of the tip vortices maintains the velocity deficit within the wake. The other modes, some of them related to the tower's vortex shedding, are instead beneficial to wake recovery, providing positive M.K.E. fluxes. These results highlight the crucial importance on the wake dynamics of the tower and nacelle, which generate low-frequency oscillations that play an fundamental role in the wake recovery process.

6. Conclusions

The present work provides a numerical analysis of the dynamics of the wake developing behind a three bladed wind turbine, for laminar inflow conditions, using the proper orthogonal decomposition (POD) of the unsteady flow field. The flow was simulated employing an LES approach, in which the rotor blades were modeled using the actuator line method, whereas tower and nacelle were modeled using an immersed boundary method. The POD was performed on velocity data sampled in a subdomain containing the wake. The convergence of the POD was assessed by considering different dataset composed of an increasing number of snapshots. A good convergence was reached for the first twelve modes which are those considered for the analysis. The most energetic POD modes are associated with the tip and root vortices shed by the blades, then two pair of modes connected with the von Kármán vortices shed by the tower and a pair harmonic of the tip vortices follow. Moreover, a Kelvin-Helmoltz-like instability was also isolated by another pair of modes. Most importantly, the last two modes show

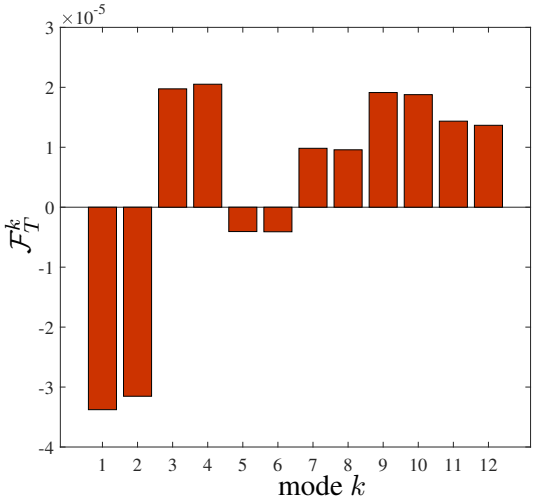

Figure 7: Turbulent mean kinetic energy fluxes per unit area $\mathcal{F}_T^k$, for the first 12 POD modes, through a cylindrical surface of radius $R = 0.5$ centered on the rotor axis.

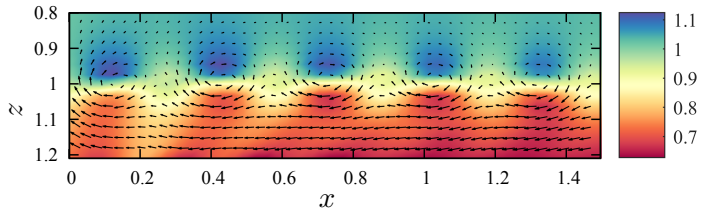

Figure 8: The shaded contours provide an x-z slice at $y = 0$ of the streamwise component of the velocity obtained as the sum of the 0^{th} mode and the first 2 modes, representing the tip vortices, each of them multiplied by the correspondent time coefficient $\mathrm{a}_k(t_1)$. The vector field is obtained by subtracting the uniform incoming flow U_∞ to the velocity field shown as shaded contours.

very large oscillations that could be related to the wake-meandering phenomenon. Finally, POD was employed to study the recovery of the wake: the contribution of each POD mode to the turbulent mean kinetic energy (M.K.E.) flux through a cylindrical surface around the wake was computed. Positive values of M.K.E. flux were found for the POD modes linked to the tower's vortex shedding, to the Kelvin-Helmholtz instability and to the wake meandering, which have, therefore, a beneficial effect on the wake recovery. On the contrary, the POD modes related to the tip vortices show negative M.K.E. fluxes, therefore they sustain the wake and slow down its recovery. The obtained results demonstrate that oscillations produced by the turbine tower affect positively the wake recovery. For this reason, neglecting the presence of tower and nacelle in the simulation of clustered turbines can lead to an underprediction of the energy production.

References

[1] Barthelmie R J, Frandsen S T, Nielsen M, Pryor S, Rethore P E and Jørgensen H E 2007 Modelling and measurements of power losses and turbulence intensity in wind turbine wakes at middelgrunden offshore wind farm *Wind Energy: An International Journal for Progress and Applications in Wind Power Conversion Technology* **10** 517–528
[2] Sanderse B, Van der Pijl S and Koren B 2011 Review of computational fluid dynamics for wind turbine wake aerodynamics *Wind energy* **14** 799–819
[3] Stevens R J and Meneveau C 2017 Flow structure and turbulence in wind farms *Annual review of fluid mechanics* **49** 311–339
[4] Porté-Agel F, Bastankhah M and Shamsoddin S 2020 Wind-turbine and wind-farm flows: A review *Boundary-Layer Meteorology* **174** 1–59
[5] Iungo G V, Viola F, Camarri S, Porté-Agel F and Gallaire F 2013 Linear stability analysis of wind turbine wakes performed on wind tunnel measurements *Journal of Fluid Mechanics* **737** 499–526
[6] Viola F, Iungo G V, Camarri S, Porté-Agel F and Gallaire F 2014 Prediction of the hub vortex instability in a wind turbine wake: stability analysis with eddy-viscosity models calibrated on wind tunnel data *Journal of Fluid Mechanics* **750** R1
[7] Iungo G V, Wu Y T and Porté-Agel F 2013 Field measurements of wind turbine wakes with lidars *Journal of Atmospheric and Oceanic Technology* **30** 274–287
[8] Aitken M L and Lundquist J K 2014 Utility-scale wind turbine wake characterization using nacelle-based long-range scanning lidar *Journal of Atmospheric and Oceanic Technology* **31** 1529–1539
[9] Sirovich L 1987 Turbulence and the dynamics of coherent structures. parts i-iii. *Quarterly of applied mathematics* **45** 561–590
[10] Berkooz G, Holmes P and Lumley J L 1993 The proper orthogonal decomposition in the analysis of turbulent flows *Annual review of fluid mechanics* **25** 539–575
[11] VerHulst C and Meneveau C 2014 Large eddy simulation study of the kinetic energy entrainment by energetic turbulent flow structures in large wind farms *Physics of Fluids* **26** 025113
[12] Ivanell S, Mikkelsen R, Sørensen J N and Henningson D 2010 Stability analysis of the tip vortices of a wind turbine *Wind Energy* **13** 705–715
[13] Sarmast S, Dadfar R, Mikkelsen R F, Schlatter P, Ivanell S, Sørensen J N and Henningson D S 2014 Mutual inductance instability of the tip vortices behind a wind turbine *Journal of Fluid Mechanics* **755** 705–731
[14] Bastine D, Witha B, Wächter M and Peinke J 2015 Towards a simplified dynamicwake model using pod analysis *Energies* **8** 895–920
[15] Bastine D, Vollmer L, Wächter M and Peinke J 2018 Stochastic wake modelling based on pod analysis *Energies* **11** 612
[16] Hamilton N, Tutkun M and Cal R B 2015 Wind turbine boundary layer arrays for cartesian and staggered configurations: Part ii, low-dimensional representations via the proper orthogonal decomposition *Wind Energy* **18** 297–315
[17] Sørensen J N, Mikkelsen R F, Henningson D S, Ivanell S, Sarmast S and Andersen S J 2015 Simulation of wind turbine wakes using the actuator line technique *Philosophical Transactions of the Royal Society A: Mathematical, Physical and Engineering Sciences* **373** 20140071
[18] Debnath M, Santoni C, Leonardi S and Iungo G V 2017 Towards reduced order modelling for predicting the dynamics of coherent vorticity structures within wind turbine wakes *Philosophical Transactions of the Royal Society A: Mathematical, Physical and Engineering Sciences* **375** 20160108
[19] Pope S B 2000 *Turbulent Flows* (Cambridge University Press)
[20] Orlandi P 2000 *Fluid flow phenomena: a numerical toolkit* (*Fluid Mechanics and Its Applications* vol 55) (Springer Netherlands)
[21] Sørensen J N and Shen W Z 1999 Computation of wind turbine wakes using combined navier-stokes/actuator-line methodology *Proc. of European Wind Energy Conference EWEC '99, Nice* pp 156–159
[22] Santoni C, Carrasquillo K, Arenas-Navarro I and Leonardi S 2017 Effect of tower and nacelle on the flow past a wind turbine *Wind Energy* **20** 1927–1939
[23] de Tullio M D, De Palma P, Iaccarino G, Pascazio G and Napolitano M 2007 An immersed boundary method for compressible flows using local grid refinement *Journal of Computational Physics* **225** 2098–2117
[24] Orlandi P and Leonardi S 2006 Dns of turbulent channel flows with two-and three-dimensional roughness *Journal of Turbulence* **7** N73
[25] Orlanski I 1976 A simple boundary condition for unbounded hyperbolic flows *Journal of Computational Physics* **21** 251–269
[26] Cal R B, Lebrón J, Castillo L, Kang H S and Meneveau C 2010 Experimental study of the horizontally averaged flow structure in a model wind-turbine array boundary layer *Journal of Renewable and Sustainable Energy* **2** 013106
[27] Segalini A and Alfredsson P H 2013 A simplified vortex model of propeller and wind-turbine wakes *Journal of Fluid Mechanics* **725** 91–116